Article

Self-Assembly, Molecular Dynamics, and Kinetics of Structure Formation in Dipole-Functionalized Discotic Liquid Crystals

Mahdy M. Elmahdy, Xi Dou, Mihail Mondeshki, George Floudas, Hans-Jürgen Butt, Hans W. Spiess, and Klaus Müllen

J. Am. Chem. Soc., **2008**, 130 (15), 5311-5319 • DOI: 10.1021/ja7113618 • Publication Date (Web): 07 March 2008

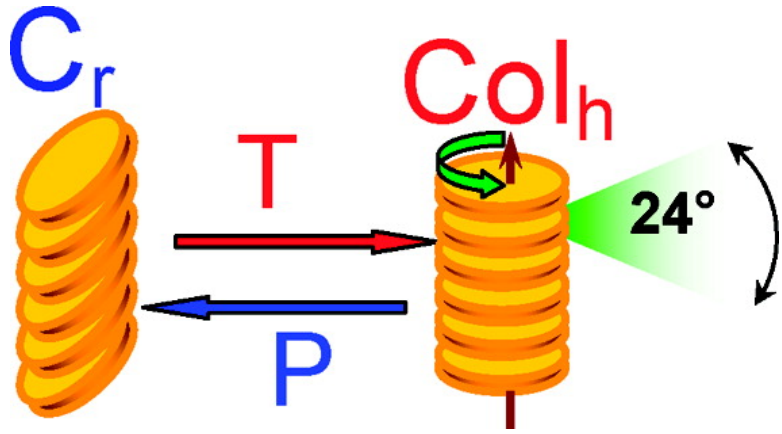

J|A|C|S
ARTICLES

Published on Web 03/07/2008

Self-Assembly, Molecular Dynamics, and Kinetics of Structure Formation in Dipole-Functionalized Discotic Liquid Crystals

Mahdy M. Elmahdy,[†] Xi Dou,[‡] Mihail Mondeshki,[‡] George Floudas,*[,†] Hans-Jürgen Butt,[‡] Hans W. Spiess,[‡] and Klaus Müllen*[,‡]

Department of Physics, University of Ioannina, 451 10 Ioannina, Greece, and Foundation for Research and Technology-Hellas (FORTH-BRI) and Max-Planck Institute for Polymer Research, 55128 Mainz, Germany

Received December 29, 2007; E-mail: gfloudas@cc.uoi.gr; muellen@mpip-mainz.mpg.de

Abstract: The self-assembly, the molecular dynamics, and the kinetics of structure formation are studied in dipole-functionalized hexabenzocoronene (HBC) derivatives. Dipole substitution destabilizes the columnar crystalline phase except for the dimethoxy- and monoethynyl-substituted HBCs that undergo a reversible transformation to the crystalline phase. The disk dynamics are studied by dielectric spectroscopy and site-specific NMR techniques that provide both the time-scale and geometry of motion. Application of pressure results in the thermodynamic phase diagram that shows increasing stability of the crystalline phase at elevated pressures. Long-lived metastability was found during the transformation between the two phases. These results suggest new thermodynamic and kinetic pathways that favor the phase with the highest charge carrier mobility.

Introduction

Conducting discotic liquid crystals have the capacity to serve as active electronic components in devices.[1] Alkyl substituted hexabenzocoronenes (HBC),[2] in particular, were found to be very promising as active semiconductors in organic field-effect transistors and photovoltaic devices. A key factor in the design of HBCs for electronic applications is the high one-dimensional charge carrier mobility (above 1 cm^2/Vs) that is approaching the value for the intersheet mobility in graphite (3 cm^2/Vs).[3,4] The origin of this favorable charge carrier mobility is the optimized $\pi-\pi$ overlap of the aromatic cores. The purpose of the alkyl chains is to introduce solubility, proccessability, and a rich thermotropic behavior. During the process of self-organization, the disk-shaped molecules organize into columns that assemble into two-dimensional arrays, whereas the alkyl chains fill the intercolumnar space.[5] The balance of enthalpic and entropic interactions is shifted in HBCs toward the former that stabilize two main columnar structures: a hexagonal liquid crystalline phase (Col_h) and a crystalline phase (C_r), at higher and lower temperatures, respectively. Nevertheless, the stability of these phases (i.e., the exact phase state) remains unknown for the majority of the compounds. In view of the high charge carrier mobility of the crystalline phase, the stability of this phase to temperature and pressure variations needs to be explored in detail.

Another, seemingly unrelated issue is that of the intrinsic disk mobility within the columnar structures. Since the electronic charge carriers are likely to be transported by the stacked HBC cores, knowledge of the intrinsic rotational dynamics of the discs is important for the design of HBCs for particular applications. In this respect, recent efforts by NMR,[6–13] dielectric spectroscopy (DS),[11–20] neutron scattering,[21,22] and computer simulations[22–24] have shed some light on the dynamics of discotic liquid crystals.

A systematic investigation of discotic liquid crystals with respect to the nanoscale self-assembly, the molecular dynamics, the thermodynamic phase state, and the pathways of structure formation with possible metastable states, requires a combination of model systems bearing dipoles directly attached to the cores

[†] University of Ioannina.
[‡] Max-Planck Institute for Polymer Research.

(1) Novoselov, K. S.; Geim, A. K.; Morozov, S. V.; Jiang, D.; Katsnelson, M. I.; Grigorieva, I.; Dubonos, S. V.; Firsov, A. *Nature (London)* **2005**, *438*, 197–200.
(2) Wu, J.; Pisula, W.; Müllen, K. *Chem. Rev.* **2007**, *107*, 718–747.
(3) Pisula, W.; Menon, A.; Stepputat, M.; Lieberwirth, I.; Kolb, U.; Tracz, A.; Sirringhaus, H.; Pakula, T.; Müllen, K. *Adv. Mater.* **2005**, *17*, 684–689.
(4) van de Craats, A. M.; Warman, J. M.; Fechtenkötter, A.; Brand, J. D.; Harbison, M. A.; Müllen, K. *Adv. Mater.* **1999**, *11*, 1469–1472.
(5) *Handbook of Liquid Crystals*; Demus, D., Goodby, J., Gray, G. W., Spiess, H.-W., Vill, V., Eds.; Wiley-VCH.: Weinheim, Germany, 1998.
(6) Leisen, J.; Werth, M.; Boeffel, C.; Spiess, H. W. *J. Chem. Phys.* **1992**, *97*, 3749–3759.
(7) Werth, M.; Leisen, J.; Boeffel, C.; Dong, R. Y.; Spiess, H. W. *J. Phys. II France* **1993**, *3*, 53–67.
(8) Hollander, A.; Hommels, J.; Prins, K. O.; Spiess, H. W.; Werth, M. *J. Phys. II France* **1996**, *6*, 1727–1741.
(9) Herwig, P.; Kayser, C. W.; Müllen, K.; Spiess, H. W. *Adv. Mater.* **1996**, *8*, 510–513.
(10) Fischbach, I.; Pakula, T.; Minken, P.; Fechtenkötter, A.; Müllen, K.; Spiess, H. W.; Saalwächter, K. *J. Phys. Chem. B* **2002**, *106*, 6408–6418.
(11) Vallerien, S. U.; Werth, M.; Kremer, F.; Spiess, H. W. *Liq. Cryst.* **1990**, *8*, 889–893.
(12) Werth, M.; Vallerien, S. U.; Spiess, H. W. *Liq. Cryst.* **1991**, *10*, 759–770.
(13) Möller, M.; Wendorff, J. H.; Werth, M.; Spiess, H. W.; Bengs, H.; Karthaus, O.; Ringsdorf, H. *Liq. Cryst.* **1994**, *17*, 381–395.
(14) Möller, M.; Wendorff, J. H.; Werth, M.; Spiess, H. W. *J. Non-Cryst. Solids* **1994**, *170*, 295–299.
(15) Ngai, K.L. *J. Non-Cryst. Solids* **1996**, *197*, 1–7.
(16) Glüsen, B.; Kettner, A.; Kopitzke, J.; Wendorff, J. H. *J. Non-Cryst. Solids* **1998**, *241*, 113–120.

Table 1. Thermal Properties and Transition Temperatures

sample	transition temperature (K)	enthalpy (J/g)	phase/phase transition[e]	d_{10} (nm)[d]	lattice parameter a (nm)[d]	d_{intra} (nm)[d]
monocyano HBC	234[a](228)[b]237[c]		Col_h/glass transition Col_h/glass transition	2.40	2.77	0.360
monobromo HBC	238[a](226)[b]237[c]		Col_h/glass transition	2.48	2.86	0.363
dimethoxy HBC	382[a](344)[b]236[c]	52[a] (54)[b]	C_r−Col_h/glass transition	2.51	2.90	0.363
monoethynyl HBC	305[a](280)[b]236[c]	24[a] (18)[b]	C_r−Col_h/glass transition	2.25	2.60	0.354

[a] Heating (differential scanning calorimetry). [b] Cooling (differential scanning calorimetry). [c] Cooling (dielectric spectroscopy). [d] At 403 K (Col_h phase). [e] C_r, crystalline phase; Col_h, columnar hexagonal liquid crystalline phase.

and different microscopic techniques that are sensitive probes of the time-scale and geometry of motion. Furthermore, additional thermodynamic variables are needed (i.e., pressure[25]) for constructing the complete phase diagram. For this purpose we employ a series of dipole-functionalized HBCs. First, we study the effect of dipole substitution on the stability of the liquid crystalline phases. Second, we investigate the core dynamics within the columns by combining dielectric spectroscopy with site-specific NMR techniques. These probes provide unambiguously the rate and geometry of motion. Third, we employ pressure and investigate, for the first time, the stability of the liquid crystalline and crystalline phases by providing the thermodynamic phase diagram for the dimethoxy-substituted HBC. This study delineates the pressure and temperature stability limits of the crystalline phase associated with the highest charge carrier mobility. Lastly, we monitor for the first time, the evolution of structure formation by dielectric means, following a distinct path within the $T-P$ phase diagram. In that study we are interested in the presence or absence of intermediate states, the possible nucleation sites, and the existence of long-lived metastability. The latter study provides glimpses of the exact mechanism for structural reorganization and growth.

Results and Discussion

Structure. The DSC traces of the monocyano and monobromo HBCs did not show a phase transformation within the investigated T-range. We observed, however, a glass temperature at 236 K (Table 1 and Figure S1, Supporting Information). In contrast, the DSC traces of the dimethoxy- (Figure 1) and monoethynyl HBCs revealed a first-order phase transformation. The single phase in the monocyano and monobromo HBCs as well as the high temperature phase in the dimethoxy- and monoethynyl HBCs exhibit similar features when examined by WAXS from extruded fibers: a set of strong meridional reflections and a set of equatorial reflections with ratios $1:3^{1/2}:4^{1/2}$ relative to the primary peak (Figure 1). The former reflect intracolumnar distances whereas the latter are of intercolumnar

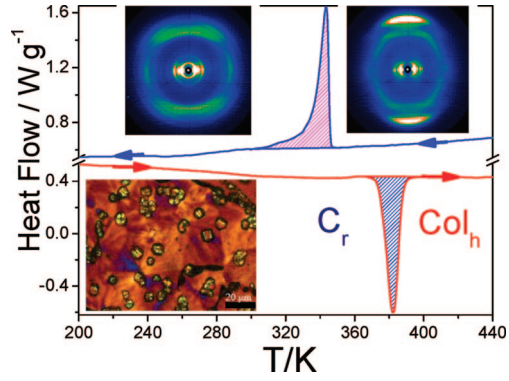

Figure 1. DSC trace of the dimethoxy HBC obtained during the second cooling/heating runs with 10 K/min: 2D WAXS images obtained from an oriented fiber shown at 303 and 373 K (the latter obtained on cooling), corresponding respectively to the crystalline (C_r) and columnar hexagonal liquid crystalline phase (Col_h). The image from POM obtained on slow cooling at 303 K shows both spherulites (C_r) with a radial columnar orientation and smaller circular objects with columnar growth around the nucleation centers (Col_h).

origin (Table 1) and correspond to the (10), (11), and (20) reflections of a hexagonal lattice. The d_{hk} spacings (where h and k are the Miller indices) are related to the lattice parameter a through the following (see Supporting Information for eqs 1−3)

$$\frac{1}{d_{hk}^2} = \frac{4}{3}\frac{h^2 + k^2 + hk}{a^2} \tag{4}$$

and suggest the formation of a columnar hexagonal liquid crystalline phase (Col_h). The calculated d-spacings and the lattice parameters are included in Table 1.

On the other hand, the low temperature phase in the dimethoxy HBC, is crystalline (C_r). As we will see later with respect to the dynamics, despite the strong WAXS reflections within C_r, the discs can still rotate. The off-meridional reflections indicate a tilt of the discotic cores with respect to the columnar axis with an intracolumnar periodicity of ~0.36 nm, giving rise to the known "herringbone" structure. As a result of the elliptic projection of the discs in the plane, the symmetry of the C_r phase deviates from the usual hexagonal lattice. The sequence of equatorial reflections appears now at wave vectors, 2.48, 3.6, and 5 nm^{-1}. A complete indexation of the C_r phase is, however, ambiguous because of the limited number of reflections and very broad peaks. A 2D rectangular or oblique unit cell has been proposed for this structure.[37,38] Within both phases the side-chains are molten as shown by the small values of the local dynamic order parameter deduced from NMR (see below) and from the absence of distinct reflections in X-rays. Their intra- and intermolecular correlations give rise to a broad "amorphous halo" centered around $q \approx 12$–14 nm^{-1}.

The $Col_h \rightarrow C_r$ transformation revealed a hysteresis (Figure 1). The WAXS images display mixed reflections on cooling to 303

(17) Yildirim, Z.; Wübbenhorst, M.; Mendes, E.; Picken, S. J.; Paraschiv, I.; Marcelis, A. T. M.; Zuilhof, H.; Sudhölter, E.J R. *J. Non-Cryst. Solids* **2005**, *351*, 2622–2628.
(18) Kruglova, O.; Mendes, E.; Yildirim, Z.; Wübbenhorst, M.; Mulder, F. M.; Stride, J. A.; Picken, S.J.; Kearley, G. J. *ChemPhysChem* **2007**, *8*, 1338–1344.
(19) Elmahdy, M. M.; Floudas, G.; Mondeshki, M.; Spiess, H. W.; Dou, X. Müllen, K. *Phys. Rev. Lett.*, 2008, in press.
(20) Elmahdy, M. M.; Floudas, G. Kastler, M. Müllen, K. Unpublished work.
(21) Kearley, G. J.; Mulder, F. M.; Picken, S. J.; Kouwer, P. H. J.; Stride, J. *Chem. Phys.* **2003**, *292*, 185–190.
(22) Mulder, F. M.; Stride, J.; Picken, S. J.; Kouwer, P. H. J.; de Haas, M. P.; Siebbeles, L. D. A.; Kearley, G. J. *J. Am. Chem. Soc.* **2003**, *125*, 3860–3866.
(23) Andrienko, D.; Marcon, V.; Kremer, K. *J. Chem. Phys.* **2006**, *125*, 124902–124909.
(24) Kirkpatrick, J.; Marcon, V.; Nelson, J.; Kremer, K.; Andrienko, D. *Phys. Rev. Lett.* **2007**, *98*, 227402–227405.
(25) Floudas, G. *Prog. Polym. Sci.* **2004**, *29*, 1143–1171.

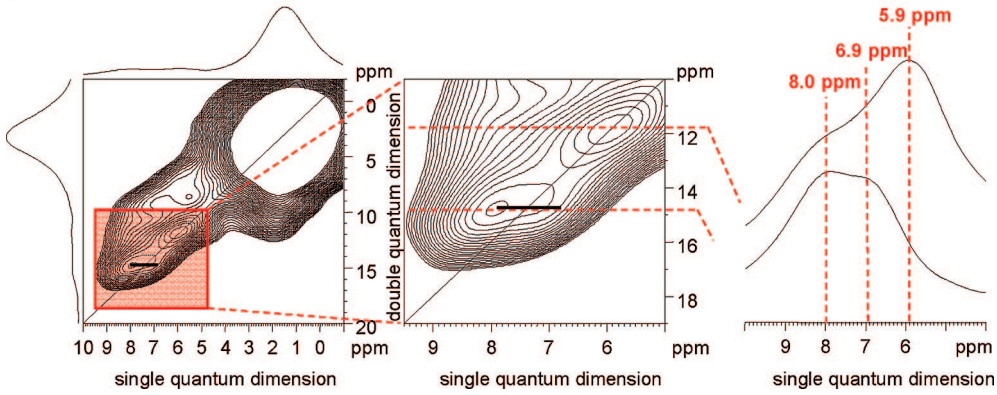

Figure 2. (Left) Two-dimensional solid-state $^1H-^1H$ DQ MAS NMR spectrum of the dimethoxy HBC recorded at 310 K (effective sample temperature), 40 μs used to excite and reconvert the DQ coherences and 25 kHz MAS; (middle) the aromatic region magnified; and (right) two one-dimensional slices at 11.8 and 14.9 ppm with the aromatic proton chemical shifts assigned.

K from the Col_h phase, suggesting a slow phase transformation (Figure S2, Supporting Information). This is also evident in the POM image of the dimethoxy HBC (Figure 1), taken at 303 K on cooling from 500 K. The image displays several circular textures with columnar growth around the multiple nucleation centers (Col_h) and some spherulitic textures with a radial columnar orientation (C_r). Note that the nucleation density of the former features exceeds the latter as well as the absence of any correlation between the nucleation sites of the Col_h and C_r phases. This phase coexistence reflects the very slow phase transformation kinetics that will be explored below.

In addition to the above scattering experiments, NMR can also be employed to identify the type of columnar packing. Recently, the comparison of quantum chemical ab initio calculations with experimental ^1H solid-state NMR spectra allowed the assignment of the specific molecular packing.[39,40] This approach takes advantage of the marked sensitivity of the ^1H chemical shift to intermolecular interactions. ^1H magic-angle spinning (MAS) and $^1H-^1H$ two-dimensional double quantum (DQ) MAS NMR experiments were performed on the dimethoxy HBC within the C_r and Col_h phases. The $^1H-^1H$ DQ MAS spectrum (Figure 2) reveals a pattern characteristic of a tilted arrangement of HBC discs (i.e., with the "herringbone" structure[39]). Three aromatic resonances within the C_r phase that could be explained by the different degrees to which the aromatic protons experience the ring current of adjacent layers are observed. These resonances merge into a single peak on heating to the Col_h phase, where the aromatic protons in the planar disk arrangement experience identical average ring currents.[40]

The effect of dipole substitution is to destabilize the C_r phase: in the HBCs bearing the stronger dipoles ($\mu_{monocyano} = 4.55$ D, $\mu_{monobromo} = 1.62$ D) the C_r phase is completely unstable, whereas in the HBCs with the weaker dipoles ($\mu_{dimethoxy} = 0.64$ D, $\mu_{monoethynyl} = 0.25$ D) the C_r phase appears at low temperatures. These results on the dipole-functionalized HBCs are in agreement with earlier studies on HBCs[26a,27] and triphenylene[41–43] discotic liquid crystals. For example, monosubstituted triphenylenes with similar polar functionalities exhibited increased stability of the liquid crystalline mesophase;[41] the C_r phase was destabilized and the range corresponding to the liquid crystalline phase was increased by some 122 K. Another study[43] explored the effect of electron-withdrawing and electron-donating groups. It was found that the former had greater propensity of forming columnar phases as compared to the latter that were essentially nonmesogenic. The type of side chains (linear vs branched) may also affect the width of the C_r and Col_h phases.[26a,44] There are two earlier studies on bromo-functionalized HBCs in the ortho and para positions bearing either linear[27] or branched[26a] chains. In both cases, that is, independent of the type of alkyl side chain, the effect of dipole substitution in the ortho position was to shift the C_r to Col_h transition to lower temperatures. In the case of para substitution, the net dipole is zero and thus the transition temperature was unaffected. This suggests that when comparing the effects of dipole substitution and type of alkyl chains it is the former that exerts the stronger influence on the phase state of the HBC compounds investigated herein. In conclusion, NMR and WAXS experiments allowed the complete identification of the two columnar phases; columnar hexagonal liquid crystalline (Col_h) and crystalline (C_r) phases at higher and lower temperatures, respectively.

Dynamics. The analysis of the heteronuclear NMR rotor encoded rotational echo double resonance NMR (REREDOR) spinning sideband patterns provides site-specific information of the molecular motion[19,31,32] through the effective $^1H-^{13}C$ dipole–dipole coupling constant, D_{CH}, and the associated local dynamic order parameter, S, representing the residual motional anisotropy of a given molecular segment. S is given in the form of the second order Legendre polynomial and is obtained experimentally as the ratio of the measured effective dipole–dipole coupling constant to that of a static pair:

$$S_{CH} = \left\langle \frac{1}{2}(3\cos^2\theta_{CH}(t) - 1) \right\rangle_t = \frac{\langle D_{CH}(t)\rangle_t}{D_{CH,static}} \qquad (5)$$

Different experiments were performed for the dimethoxy HBC derivative, corresponding to the C_r and Col_h phases. For quantitative analysis the recorded REREDOR spinning sideband

(26) (a) Fechtenkötter, A.; Tchebotareva, N.; Watson, M.; Müllen, K. *Tetrahedron* **2001**, *57*, 3769–3783. (b) Dou, X.; Yang, X.; Bodwell, G. J.; Wagner, M.; Enkelmann, V.; Müllen, K. *Org. Lett.* **2007**, *9*, 2485–2488.
(27) Ito, S.; Wehmeier, M.; Brand, J. D.; Kübel, C.; Epsch, R.; Rabe, J. R.; Müllen, K. *Chem. Eur. J.* **2000**, *6*, 4327–4342.
(28) Wu, J.; Qu, J.; Tchebotareva, N.; Müllen, K. *Tetrahedron Lett.* **2005**, *46*, 1565–1568.
(29) Feike, M.; Demco, D. E.; Graf, R.; Gottwald, J.; Hafner, S.; Spiess, H. W. *J. Magn. Reson.* **1996**, *A 122*, 214–221.
(30) Schnell, I.; Spiess, H. W. *J. Magn. Res., Adv. Magn. Reson.* **2001**, *151*, 153–227.
(31) Saalwächter, K.; Schnell, I. *Solid State Nucl. Magn. Reson.* **2002**, *22*, 154–187.
(32) Saalwachter, K.; Spiess, H. W. *J. Chem. Phys.* **2001**, *114*, 5707–5728.

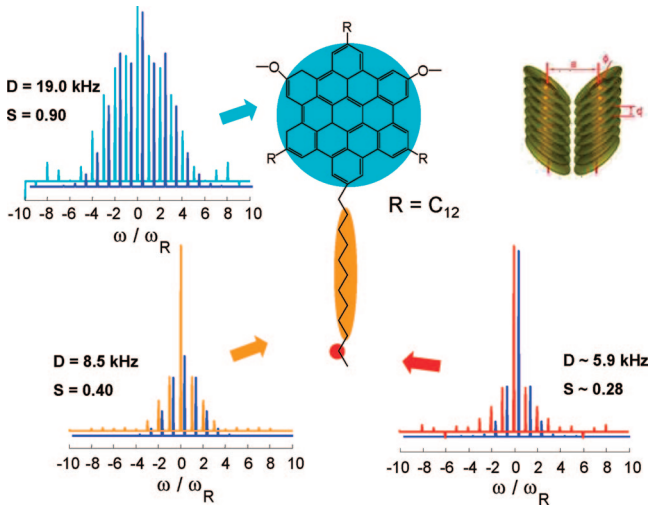

Figure 3. NMR REREDOR spinning sideband patterns for the dimethoxy HBC recorded at 25 kHz spinning at the magic angle, 80 μs recoupling time, and 310 K effective sample temperature in the crystalline state (C_r), with the calculated patterns (in blue) superimposed. The derived $^1H-^{13}C$ dipole–dipole coupling constants for the respective CHn ($n = 1, 2$) moieties are presented together with the related local dynamics order parameters, respectively, for the HBC core $S = 0.90$ (top, left), the alkyl chains $S = 0.40$ and the more mobile chain ends $S \approx 0.28$ (middle). The typical herringbone structure is also shown (top, right)

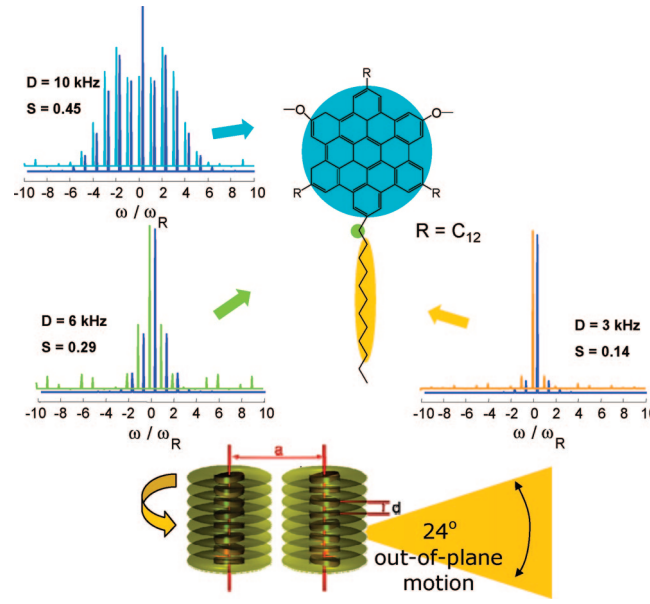

Figure 4. NMR REREDOR spinning sideband patterns for the dimethoxy HBC recorded at 25 kHz spinning at the magic angle, 160 μs recoupling time and 400 K effective sample temperature in the liquid-crystalline state (Col_h), with the calculated patterns (in blue) superimposed. The derived $^1H-^{13}C$ dipole–dipole coupling constants for the respective CHn ($n = 1$, 2) moieties are presented together with the related local dynamics order parameters S. Note that the aromatic core S-value is reduced to 0.45 suggesting both in-plane rotation and out-of-plane excursions, while the higher degree of motional freedom for the alkyl chains results in S values in the range of 0.29 to 0.14. The columnar disk organization within the Col_h phase is shown in the bottom.

patterns are compared with calculated ones for different dipole–dipole coupling constants. The fit has an estimated accuracy of 10%. The intensity of the center-band, being sensitive to multispin effects, is typically not included in the analysis. In the crystalline state (Figure 3), the measured $^1H-^{13}C$ dipole–dipole coupling constant for the aromatic CH pairs is ca.19 kHz ($S = 0.90$) showing that the aromatic core is essentially rigid at 310 K. The slight reduction of the $^1H-^{13}C$ dipole–dipole coupling constant from the rigid state value (i.e., $S = 1$) can be due to in-plane fluctuations as well as to out-of-plane disk excursions. On the contrary, the C12 alkyl chains retain significant mobility within the crystalline state. The effective dipole–dipole coupling constants measured for the chain CH_2 groups ($D = 8.5$ kHz, $S = 0.40$) and at the chain ends ($D \approx 5.9$ kHz, $S \approx 0.28$) clearly show that on average the C12 chains remain flexible and amorphous. Therefore within the crystalline phase, discs are not completely frozen but are able to perform small-angle motions, whereas the alkyl chains retain significant mobility.

In the Col_h mesophase, the $^1H-^{13}C$ dipole–dipole coupling constant for the aromatic CH moiety of the dimethoxy HBC first of all, is reduced by a factor of 2 because of the fast in-plane rotation of the discotic molecules similar to ^2H NMR, where the same bond direction is probed.[6,9–12,19] Further reduction of the dynamic order parameter of the core CH segment ($S = 0.45$) is attributed to out-of-plane disk excursions. The mean angle (24°) of the latter (Figure 4) is determined by assuming that the local dynamic order parameter S results from a Gaussian orientation distribution of displacement angles.[45] In the Col_h mesophase the alkyl chain dynamics exhibits a mobility gradient from the spatially most restricted Cα CH_2 group ($D = 6.0$ kHz, $S = 0.29$) to the more distant alkyl groups ($D = 3.0$ kHz, $S = 0.14$).

With respect to the monocyano- and monobromo-functionalized HBCs possessing the same structure (Col_h), similar results were obtained: a glassy phase at temperatures below 240 K, where the aromatic core is practically frozen ($D = 21.0$ kHz, $S \rightarrow 1$). This temperature lies in the proximity of the glass temperature identified by DS (Table 1). At higher temperatures, the $^1H-^{13}C$ dipole–dipole coupling constant of the aromatic CH moiety is 8.8 kHz. Thus, within the Col_h phase of the monocyano HBC derivative, the disk dynamics is characterized by larger out-of plane excursions ($\sigma = 38°$), as compared to the dimethoxy derivative. Nevertheless, for all compounds within the Col_h phase the main relaxation process reflects

(33) Langer, B.; Schnell, I.; Spiess, H. W.; Grimmer, A.-R. *J. Magn. Reson.* **1999**, *138*, 182–186.
(34) Havriliak, S.; Negami, S. *Polymer* **1967**, *8*, 161.
(35) *Broadbend Dieletcric Spectroscopy*; Kremer, F., Schönhals, A., Eds.; Springer: Berlin, 2002.
(36) Pakula, T. In *Broadbend Dieletcric Spectroscopy*; Kremer, F., Schönhals, A., Eds.; Springer: Berlin, 2002.
(37) Kumar, S. *Chem. Soc. Rev.* **2006**, *35*, 83.
(38) Laschat, S.; Baro, A.; Steinke, N.; Giesselmann, F.; Hägele, C.; Scalia, G.; Judele, R.; Kapatsina, E.; Sauer, S.; Schreivogel, A.; Tosoni, M. *Angew. Chem., Int. Ed.* **2007**, *46*, 4832.
(39) Ochsenfeld, C.; Brown, S.; Schnell, I.; Gauss, J.; Spiess, H. W. *J. Am. Chem. Soc.* **2001**, *123*, 2597–2606.
(40) Brown, S.; Schnell, I.; Brand, J. D.; Müllen, K.; Spiess, H. W. *J. Am. Chem. Soc.* **1999**, *121*, 6712–6718.
(41) Rego, J. A.; Kumar, S.; Ringsdorf, H. *Chem. Mater.* **1996**, *8*, 1402.
(42) Boden, N.; Bushby, R. J.; Cammidge, A. N.; Duckworth, S.; Headdock, G. J. *Mater. Chem.* **1997**, *7*, 601. (a) Boden, N.; Bushby, R. J.; Lu, Z. B.; Cammidge, A. N. *Liq. Cryst.* **1999**, *26*, 495.
(43) Foster, E. J.; Jones, R. B.; Lavigueur, C.; Williams, V. E. *J. Am. Chem. Soc.* **2006**, *128*, 8569.
(44) Liu, C.-Y.; Fechtenkötter, A.; Watson, M. D.; Müllen, K.; Bard, A. J. *Chem. Mater.* **2003**, *15*, 124.
(45) Schmidt-Rohr, K.; Spiess, H. W. *Multidimensional Solid State NMR and Polymers*; Academic Press: New York, 1994.

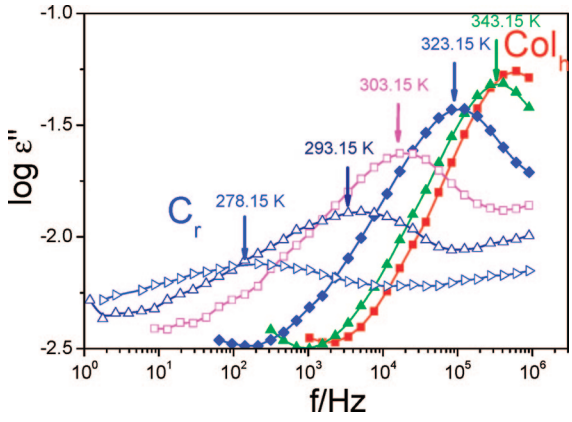

Figure 5. Dielectric loss for the dimethoxy HBC obtained on cooling at 0.1 MPa, shown at different temperatures: (filled squares) 353.15 K, (filled up triangles) 343.15 K, (filled rhombus) 323.15 K, (open squares), 303.15 K, (open up triangles), 293.15 K and (open right triangles), 278.15 K. Notice the loss in dielectric strength and the broadening of the relaxation spectrum on entering the C_r phase. The spectrum at 343.15 K corresponds to the DSC exotherm, and the one at 303.15 K is the critical temperature suggested by DS.

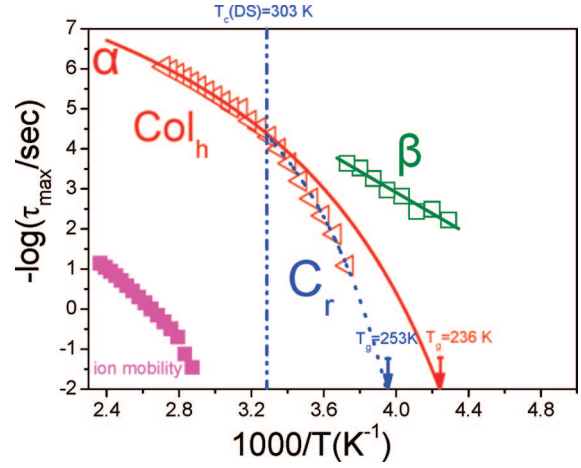

Figure 6. Temperature dependence of the relaxation times (obtained on cooling) for all dielectrically active processes and of the ionic mobility in the dimethoxy HBC: (filled squares) ionic mobility, (open squares) β-process, (left triangles) α-process. Notice the change in the α-process dynamics in going from the high temperature Col_h to the C_r phase (vertical dashed-dotted line). Full and dotted lines extrapolate to the glass temperature (defined at $\tau \approx 10^2$ s) of the Col_h (hypothetical) and C_r phases, respectively.

coupled in-plane and out-of-plane disk motions over the whole temperature range.[19]

The corresponding time-scales can best be studied in the HBCs bearing strong dipole moments through dielectric spectroscopy. Since the dipoles are directly attached to the core, the disk dynamics can be probed and compared directly with the core dynamics obtained by NMR. We discuss first the molecular dynamics of the dimethoxy HBC that undergoes a transformation from the crystalline to the columnar hexagonal liquid crystalline phase. Figure 5 depicts a series of dielectric loss curves measured at different temperatures, both below and above the transition, reflecting the in-plane disk rotation (α-process). The curves show increasing broadening and a reduction in the dielectric strength in going from the high temperature Col_h phase to the C_r phase. Note that the DSC crystallization temperature (at 343 K) is substantially higher than the one assigned by DS (at 303 K; based on the broadening of the loss curves) reflecting a strong rate dependence of the critical temperature T_c. The Figure also depicts a faster process known as β-process.

The relaxation times of the different processes in the dimethoxy HBC are shown in Figure 6, in the usual Arrhenius representation. The low-temperature β-process has an Arrhenius $\tau(T)$ dependence

$$\tau = \tau_0 e^{E/RT} \tag{6}$$

with a single activation energy $E = 50 \pm 4$ kJ/mol and $\tau_0 = 4 \times 10^{-14}$ s, characteristic of a local process associated with small amplitude vibrations (dielectric strength of only $T\Delta\epsilon \approx 7$ K) within the C_r phase. A broad distribution of relaxation times is evident by the values of the HN shape parameters ($m = mn = 0.3$). The mere presence of this process does not contradict the NMR result ($S = 1$, within C_r) because the averaging of the $^{13}C-^{1}H$ dipole–dipole couplings requires motions on a time scale faster than 10^{-5} s.

Two-dimensional exchange NMR is able, however, to unravel the geometry of motions on longer time-scales.[6,45] On the basis of the combined information from NMR (geometry of motion) and DS (rates of motion), the α-process reflects collective axial disk motions around the columnar axes. The α-process displays unique characteristics in going from the C_r to the Col_h phase. Within the Col_h phase, the $\tau(T)$ dependence can be described by the Vogel–Fulcher–Tammann (VFT) equation

$$\tau = \tau_0 \exp\left(\frac{B}{T - T_0}\right) \tag{7}$$

where τ_0 ($\sim 6 \times 10^{-6}$ s within the Col_h phase) is the relaxation time in the high T limit, B is the activation parameter, and T_0 is the "ideal" glass temperature. The B, T_0, and T_g (the glass temperature is identified as the temperature where the corresponding structural relaxation time is at 10^2 s) parameters assume the following values: 1345 ± 50, 185 ± 7, and 236 ± 7 K, respectively. On entering the C_r phase, the α-process displays a steeper T-dependence with B, T_0 and T_g parameters assuming values of 1013 ± 2 K, 214 ± 4 K and 253 ± 4 K, respectively. Notice that the crystalline phase has a higher effective glass temperature (corresponding to the freezing of the axial disk rotation) as compared to the (hypothetical) T_g of the Col_h phase. The Figure contains also a process due to the ionic mobility extracted from the electric modulus representation. This process is about 7 orders of magnitude slower from the α-process dynamics but bears a similar VFT temperature dependence. This suggests that the dynamics of ionic impurities, present in all HBCs, are affected by the disk rotational dynamics.

The HN shape parameters for the α-process are also sensitive indicators for the phase transformation (i.e., Figure 5). Figure 7 depicts the low- (m) and high- (mn) frequency slopes of the α-process as a function of temperature. The plot shows a narrow, albeit non-Debye process ($m = mn = 0.9$) within the Col_h phase and a much broader ($m = mn \approx 0.3$) distribution within the C_r phase. Therefore, the axial disk motion within the crystalline state is a collective process characterized by a heterogeneous environment, which gives rise to the broad distribution of relaxation times.[19] The onset of the broadening coincides with the DSC transition on cooling, however the transition, as seen from DS (assigned to the temperature where the width of the α-process doubles its high T value), appears at even lower temperatures ($T_c^{DS} \approx 303$ K), implying kinetic effects.

In Figure 8, the axial disk dynamics (comprising both in- and out-of-plane motions) are compared for the four dipole-

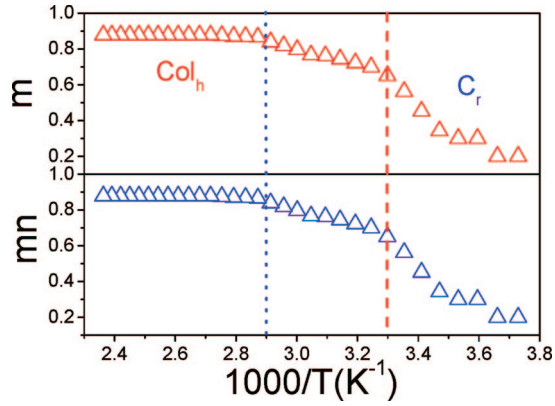

Figure 7. Temperature dependence of the low- (*m*) and high- (*mn*) frequency slopes characterizing the distribution of relaxation time spectrum of the α-process. Dotted and dashed lines give the critical temperatures of the Col_h to C_r transformation as seen from DSC and DS, respectively.

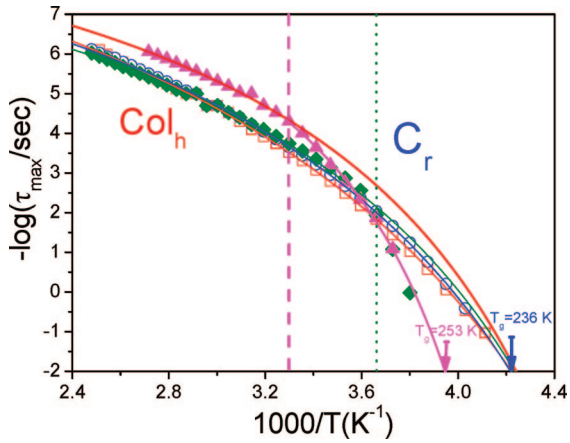

Figure 8. Comparison of the α-process relaxation times for the different dipole-functionalized discotics: (open squares) monocyano HBC, (open circles) monobromo HBC, (filled rhombus) monoethynyl HBC, and (filled up triangles) dimethoxy HBC. Notice the similarity in the $\tau(T)$ dependence within the Col_h phase and the steeper $\tau(T)$ within the C_r phase for the dimethoxy- (thick vertical line) and monoethynyl HBC (dotted vertical line).

functionalized HBCs. Within the Col_h phase, the $\tau(T)$ dependencies are nearly indistinguishable. In addition, there is no remarkable change in the distribution of relaxation times, reflecting that the phase state (Col_h) largely controls both the $\tau(T)$ and the distribution of relaxation times. From the VFT dependence of the α-process, the glass temperature assumes similar values for the three HBCs, in the range 235–237 K. The nearly indistinguishable $\tau(T)$ dependencies for the three samples within the same phase (Col_h) suggest that the timescale of the collective axial disk motion depends on *T, P,* and only weakly on alkyl chain branching. On the other hand, for the dimethoxy- and monoethynyl HBCs undergoing a transition to the crystalline state, the temperature dependence $\tau(T)$ becomes much stronger on entering the C_r phase. This again suggests that the dynamics are controlled—to a large extent—by the thermodynamic state. Last, we mention that a slower process than the α-process has been identified in the same dipole-functionalized HBCs bearing the stronger dipoles (monocyano and monobromo). The origin of this slower process has been assigned to collective reorganization of the columns, necessary to completely relax the dipole moment and pertinent, for example, to the alignment of the columns on surfaces.[19]

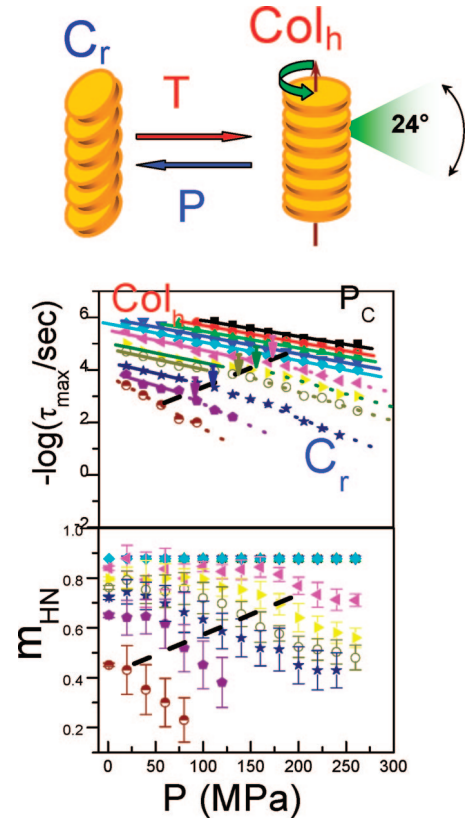

Figure 9. (Top) Schematic of the transformations between the crystalline and columnar liquid crystal phases induced by temperature and pressure. (Middle) α-Process relaxation times as a function of pressure for the following "isotherms": (filled squares) 393.15 K, (filled circles) 383.15 K, (filled up triangles) 373.15 K, (filled down triangles) 363.15 K, (filled rhombus) 353.15 K, (filled left triangles) 343.15 K, (filled right triangles) 333.15 K, (open circles) 323.15 K, (stars) 313.15 K, (filled polygons) 303.15 K and (half-filled circles) 293.15 K. Lines represent linear fits to the respective regimes. The dashed black line gives the critical pressure (P_c) for the Col_h—C_r transformation. (Bottom) HN low-frequency parameter of the α-process as a function of pressure for the different isotherms (as above). The black dashed line gives again the critical pressure P_c.

Phase State. Applications of HBCs as advanced electronic materials require knowledge of the thermodynamic temperature and pressure boundaries (spinodals) and stability (and metastability) of the different phases. In this section we aim at constructing the complete phase diagram ($P-T$) for the dimethoxy HBC that comprises different phases (Col_h, C_r, "glassy"). Hence, pressure is employed as the additional thermodynamic parameter. In these experiments, pressure is applied isothermally at temperatures corresponding to the Col_h phase where the α-process is probed within the experimental window (Figure 9). Increasing pressure first slows-down the α-process (as anticipated by densification), and subsequently induces the transformation to the C_r phase. The transformation is evident by the steeper $\tau(P)$ dependence within C_r and from the increased broadening of the α-process. The low-frequency HN parameter is included in Figure 9 and depicts a dramatic pressure-induced broadening under isothermal conditions. Thus the critical pressure, P_c, required for the transformation, can be obtained either from the change in the $\tau(P)$ dependence or from the $m(P)$ dependence and is depicted by the thick line in Figure 9.

Under the assumption that the α-process is purely activated, the linear dependence of log τ versus P can be used to extract the apparent activation volume, $\Delta V^{\#}$, as[25]

$$\Delta V^{\#} = 2.303RT\left(\frac{\partial \log \tau}{\partial P}\right)_T \quad (8)$$

According to this picture, $\Delta V^{\#}$ represents the difference between the molar volumes of the initial and final (activated) states. Nevertheless, certain similarities of this quantity with the molecular volume were found in a series of studies. This quantity, within the Col_h and C_r phases, is plotted in Figure 10 as a function of temperature and reveals a higher apparent activation volume for the α-process within the C_r phase. This is also the case in crystallizing polymers and suggests a more cooperative disk rotation within the C_r phase.[46] The apparent activation volume at 303 K (i.e., at T_g + 50 K) within the crystalline phase is about half-the molecular volume (250 cm^3/g obtained from X-rays[27]).

On the basis of the*T*- and *P*-investigations the phase diagram can be constructed for the dimethoxy HBC and is depicted in Figure 10. The figure contains the pressure dependence of the glass temperature corresponding to the freezing of the disk axial motion within the crystalline phase and the pressure dependence of the critical temperature, T_c, for the Col_h to C_r transformation obtained from the data of Figure 9. The former can be described by the empirical equation[47]

$$T_g(P) = T_g(0)\left(1 + \frac{b}{c}P\right)^{1/b} \quad (9)$$

where $T_g(0)$ = 253 K, b and c are fitting parameters ($b = 6 \pm 1$, $c = 810 \pm 90$ MPa and $(dT/dP)_{P\to 0} = 0.3$ K/MPa). The latter is described by the Clausius−Clapeyron equation for first order transitions as

$$\frac{dP}{dT} = \frac{\Delta H_f}{T\Delta V} \quad (10)$$

where ΔH_f is the heat of fusion associated with the C_r to Col_h phase transformation, T is the transition temperature at atmospheric pressure, and ΔV is the associated change of specific volume. From the slope of the $T(P)$ dependence, dP/dT = 3.6 MPa/K, and the DSC heat of fusion (54 J/g) the change of specific volume at the transition can be estimated. The thus estimated change of specific volume (0.047 cm^3/g) suggests a substantial volume reduction on entering the crystalline phase. These dependencies separate the $T-P$ phase space in three regimes depicted as "glass", "C_r" and "Col_h". As a result of the stronger pressure dependence of the first order C_r to Col_h phase transformation, as opposed to the weaker $T_g(P)$, increasing pressure effectively stabilizes the C_r phase. For example, the crystalline phase can be stabilized to 450 K at 600 MPa, that is, about 150 K above its atmospheric pressure limit. This stabilization of the crystalline phase to higher temperatures can have consequences in applications in view of the higher charge carrier mobility found in this phase.

Kinetics of Phase Transformation. The WAXS and POM investigations provided evidence for long-time Col_h-C_r coexistence on cooling from the Col_h phase. Important issues involved in phase transformation kinetics[48] include the existence of intermediate states, the identification of nucleation sites, and

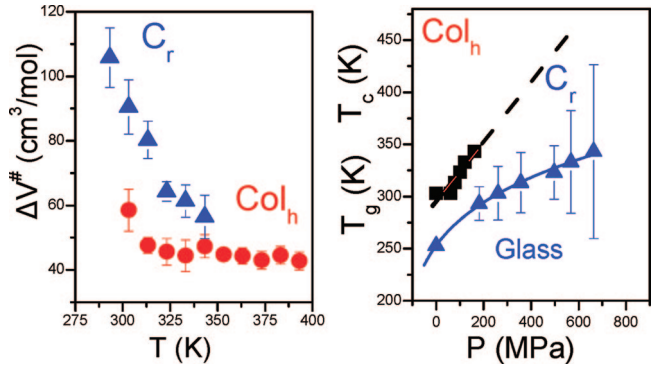

Figure 10. (Left) Temperature dependence of the apparent activation volume corresponding to the crystalline (C_r) and columnar hexagonal liquid crystalline (Col_h) phases of the dimethoxy HBC; (right) phase diagram for the dimethoxy HBC depicting the pressure dependence of the Col_h-C_r transition temperature (squares) and of the glass temperature (up triangles), the latter defined as the temperature where the α-relaxation times are at ~1 s. The lines represent fits to eqs 10 and 9, respectively.

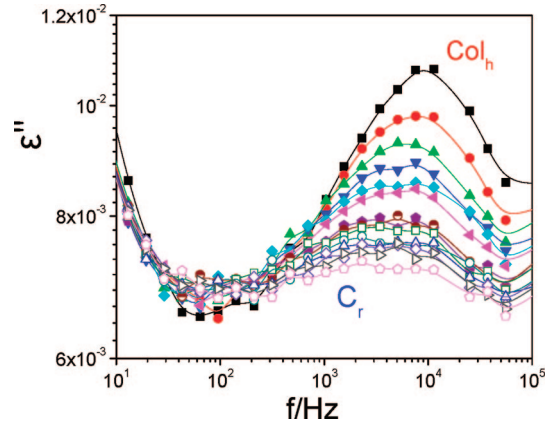

Figure 11. Kinetics of the Col_h-C_r transition for the dimethoxy HBC at 313.15 K, following a pressure jump from 0.1 to 110 MPa. The different symbols correspond to different dielectric loss curves obtained at the following times: (filled squares) 64 s, (filled circles) 118 s, (filled up triangles) 240 s, (filled down triangles) 346 s, (filled rhombus) 459 s, (filled left triangles) 570 s, (filled polygon) 1102 s, (half-filled circle) 1214 s, (open square) 1335 s, (open circle) 1803 s, (open up triangle) 1988 s, (open rhombus) 2433 s, (open right triangle) 3065 s, (open polygon) 4397 s. Notice the long time required for the transformation at this pressure.

the presence of long-lived metastability. With respect to the nucleation sites, POM (Figure 1) revealed a lower nucleation density for the crystalline phase and the absence of any correlation between the nucleation sites of the two phases. In this section we explore the effect of pressure on inducing the Col_h-C_r transformation under "isothermal" conditions. Such pressure-jump experiments are more efficient than the corresponding temperature-jump experiments since the application and equilibration of pressure is faster. Figure 11 gives the dielectric loss of the dimethoxy HBC at 313.15 K following a pressure jump from 0.1 to 110 MPa. The figure depicts the evolution of the α-process associated with the disk axial motion during the Col_h-C_r phase transformation. During the phase transformation the α-process broadens and looses dielectric strength reflecting the restricted amplitude of the in-plane and out-of-plane angular excursions within the crystalline phase (from S = 0.45 to S = 0.9). Note that the complete phase transformation requires several hours at this pressure. To explore the phase transformation kinetics, different pressure jumps have

(46) Mierzwa, M.; Floudas, G.; Stepanek, P.; Wegner, G. *Phys. Rev. B* **2000**, *62*, 14012–14019.
(47) Drozd-Rzoska, A.; Rzoska, S. J.; Imre, A. R. *J. Non-Cryst. Solids* **2007**, *353*, 3915–3923.
(48) Hadjichristidis, N.; Pispas, S.; Floudas, G. *Block Copolymers: Synthetic Strategies, Physical Properties and Applications*; Wiley & Sons Inc.: Hoboken, NJ, 2002.

Scheme 1. Schematic Structures of the Monocyano HBC (Upper Left), Monobromo HBC (Upper Right), Dimethoxy HBC (Bottom Left), and Monoethynyl HBC (Bottom Right)

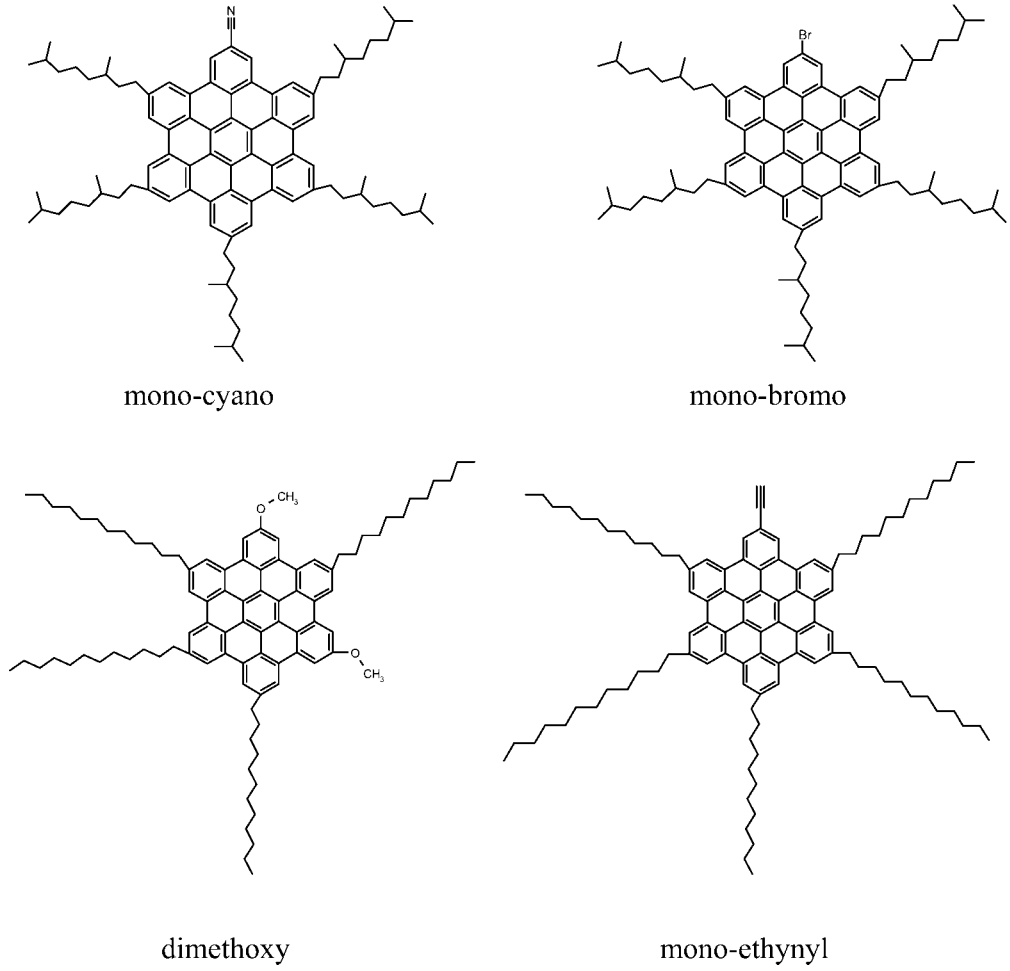

been performed starting from 0.1 MPa to different final pressures of 80, 110, 160, and 200 MPa at 313.15 K. In all cases the evolution of the integrated intensity can be represented by the well-known Kohlrausch–Williams–Watts (KWW) equation[35]

$$\int \epsilon'' \mathrm{d}f = A \exp\left[-\left(\frac{t-t_0}{\tau*}\right)^{\beta}\right] + d \qquad (11)$$

where A is the amplitude, t_0 is an initial time required for temperature equilibration following the pressure jump, τ^* is the characteristic time associated with the Col_h to C_r transformation, β is the KWW exponent, and d is a constant. The evolution of the integrated intensity is shown in Figure 12 for the different final pressures (P_f). The average characteristic times associated with the phase transformation ($\langle\tau^*\rangle = (\tau^*/\beta)\Gamma(1/\beta)$, where Γ is the gamma function) are shown in the inset and reveal that the deeper the pressure jump the faster the transformation to the C_r phase.[49] This was anticipated in crossing the Col_h−C_r spinodal, since the driving force for nucleating the new phase is expected to scale with the dimensionless parameter $\delta \approx (P - P_c)/P_c$, where P_c is the critical pressure (~60 MPa at 313.15 K). Furthermore, according to a simple nucleation and growth theory, the nucleation barrier $\Delta F/k_BT$ should scale as δ^{-2} (δ^{-1}) for homogeneous (heterogeneous) nucleation. What was not anticipated, however, is the stretched exponential relaxation (β = 0.31, 0.34, 0.46, and 0.3 for final pressures of 80, 110, 160, and 200 MPa) typical for melt relaxation dynamics. Typical nucleation and growth, proceeds via the well-known Avrami equation,[50] that is, similar to eq 11, but with exponent $\beta \geq 1$ that characterizes the type of nucleation process and the dimensionality of growth (herein the expected value of β was

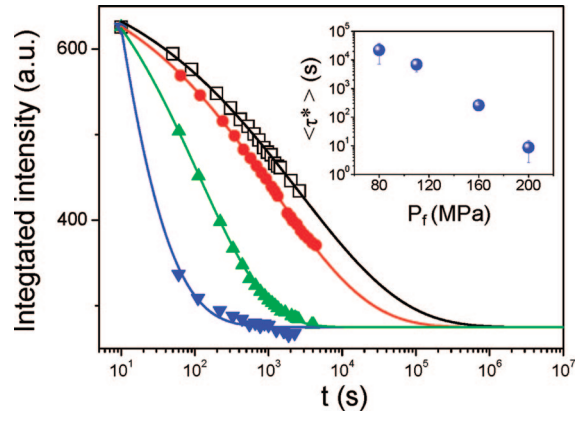

Figure 12. Evolution of the normalized integrated intensity of the α-process at 313.15 K following pressure jumps from 0.1 MPa to different final pressures: 80 MPa (open squares), 110 MPa (filled circles), 160 MPa (up triangles), and 200 MPa (down triangles). The lines are fits to eq 11. In the inset the average relaxation times are plotted as a function of final pressure (P_f).

(49) Mierzwa, M.; Floudas, G. *IEEE Trans. Dielectr. Electr. Insul.* **2001**, *8*, 359–364.

1 or 2 based on one-dimensional growth from athermal or thermal nuclei, respectively). In addition, a linear dependence of ln τ versus δ^{-2} or δ^{-1} could not be obtained. These deviations from typical nucleation and growth kinetics need to be explored in more detail, both by DS and NMR, and may reflect a more complicated scenario (e.g., fractal-type process). Nevertheless, these experiments reveal slow kinetics of phase transformation that could be important in the design of HBCs for particular applications. For example, a metastable crystalline phase can be induced for several hours by suitable pressure (or temperature) variations.

Conclusions

The self-assembly and the disk dynamics within the columnar phases were studied in a series of dipole-functionalized HBCs. The effect of functionalization with strong dipoles is to destabilize the columnar crystalline phase (C_r). On the other hand, substitution by weaker dipoles (dimethoxy- and monoethynyl HBCs) gives rise to the crystalline phase on cooling.

The disk dynamics and geometry of motion were studied by dielectric spectroscopy and site-specific NMR techniques. It was shown that the strongly temperature dependent α-process reflects the collective axial disk rotational dynamics. The glass temperature, associated with the freezing of the collective axial disk motion, was around 236 K for the discotics within the liquid crystalline phase and at 253 K for the dimethoxy-functionalized HBC within the crystalline phase. Hence, the phase state controls the dynamic response. The relaxation times and breadth of the α-process have distinctly different temperature and pressure dependencies on entering the crystalline state. These features enabled the construction of the complete phase diagram ($T-P$) for the dimethoxy-functionalized HBC. The main outcome from this study is the increased stability of the crystalline phase at elevated pressures. As a result, this phase is stabilized up to 450 K when pressurized to 600 MPa, with possible consequences with respect to charge carrier mobilities.

The transformation of the Col_h to the C_r phase, studied by pressure jumps, revealed long-lived metastability and fractional exponents that strongly depend on the quench depth. These results on the slow Col_h to C_r transformation and the stabilized C_r phase at elevated pressures suggest new thermodynamic and kinetic pathways of stabilizing the phase with the high charge carrier mobility.

Acknowledgment. The research is supported by the Greek GSRT/PENED03 and EPEAEK/YPEPTH/PYTHAGORAS I programs, the EU project NAIMO Integrated Project NMP4-CT-2004-500355, the Deutsche Forschungsgemeinschaft (DFG) in the frame of the Sonderforschungsbereich (SFB) 625, and the Max Planck Society. M.M.E. is supported by an IKY state fellowship. Discussions with Dr. D. Andrienko and Prof. K. Kremer (MPI-P) are gratefully acknowledged.

Supporting Information Available: A Materials and Methods section containing the procedures for the preparation and full characterization of all compounds is provided. Differential scanning calorimetry (DSC) traces for all compounds as well as details on polarizing optical microscopy, X-ray scattering, solid state NMR spectroscopy, and dielectric spectroscopy are provided. This material is available free of charge via the Internet at http://pubs.acs.org.

JA7113618

(50) Avrami, M. J. *J. Chem. Phys.* **1939**, *7*, 1103−1112; **1940**, *8*, 212–224; **1941**, *9*, 177–184.